Original Article

An Efficient Meningioma Tumor Segmentation System in WMSN Using UNET-RCNN Classification Approaches

John Nisha Anita[1], Dr. Sujatha Kumaran[2]

1 Research Scholar, Department of Electronics and Communication Engineering,
Sathyabama Institute of Science and Technology, Chennai.

2 Professor, Department of Electrical and Electronics Engineering,
Sathyabama Institute of Science and Technology, Chennai.

DOI: 10.47750/pnr.2023.14.03.225

Abstract

Meningioma is the primary type tumors which spreads in different regions of human brain and can be screened using Magnetic Resonance Imaging (MRI) modality method. This paper proposes an efficient framework for the detection and diagnosis of tumor regions in Meningioma brain MRI images. The proposed work is structured into two phases as tumor detection phase and tumor diagnosis phase. The tumor detection phase consists of UNet-Convolutional Neural Networks (CNN) architecture, which performs both classification and tumor region segmentation process. The features are computed from the tumor region segmented image and the computed features are used for the diagnosis of segmented tumor regions into either Early or Severe. The proposed Meningioma tumor detection methods are tested and validated on two different brain image datasets NU and Kaggle in this paper. The segmented tumor regions in meningioma brain images are transferred to the remote unit through the Wireless Multimedia Sensor Networks (WMSN).

Keywords: Meningioma, brain, tumor, segmentation, features.

1. INTRODUCTION

The tumor cells are developed due to the abnormality during the cell division process in human body with respect to various organs. The tumor cells may be occurred with respect to brain, liver, lung, breast and any parts of the human body. Among these tumors in human body, brain tumors are the most important one in and around the world. Brain tumors affect the all age groups and all kind of sex. Therefore, it is very important to screen the tumor regions in human brain to save the human life on time. Based on the location and other morphological parameters, the brain tumors are categorized into either benign or malignant. The benign cells are otherwise called as non-cancerous cells and the malignant cells are otherwise called as cancerous cells. The benign cells may be converted into malignant cells if it is not properly diagnosed on time. The spreading capacity of the malignant cells is higher in human brain when compared with spreading capacity op the benign cells. Further, the malignant cells are identified using the progression property with respect to the other surrounding cells in the human brain. Meningioma tumors are started in human brain and spread over the region of spinal cord. Other types of the brain tumors start and end with in the brain. Hence, the meningioma tumors are most important than the other types of the tumors in brain. The patient survival rate in meningioma tumor case is based on the tumor size and its severity. The meningioma tumor with 5 cm diameter size requires surgery to save the patient's life. In this paper, the meningioma tumors are detected in Magnetic Resonance Imaging (MRI) (as illustrated in Figure 1) method using deep learning approach.

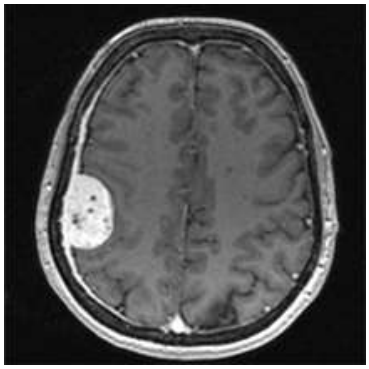

Figure 1: Meningioma case image

This paper is structured as separate internal modules as section 2 deals the existing Meningioma detection methods, section 3 presents the Meningioma grading system as proposed work, the experimental analysis of the Meningioma grading system is depicted in Section 4 and the finally the summarize the experimental results.

2. LITERATURE SURVEY

Ali et al. (2022) devised multi model abnormality detection system using comprehensive algorithm in this work. The authors surveyed high number of conventional meningioma brain tumor detection models with respect to their experimental results. The limitations of the existing methods were discussed with the point of simulation results and datasets in this work. Shanaka Ramesh et al. (2021) provided a systematic solution for meningioma tumor region detection. The authors proposed active contour based deep learning method for detecting the region of abnormal. Further, proposed active contour modeling flow segmented the abnormalities using deep learning output image. Finally, 95.9% of sensitivity, 96.1% of specificity and 96.7% of meningioma tumor image segmentation rate was attained using their active contour based deep learning model in this work. Laukamp et al. (2020) compared the tumor region segmentation output model between the automated computer methodology and the manual tumor region segmentation model in this work. The segmented region of pixels between these two approaches was pixel level fused to verify the significant of abnormal region segmentation results in this work. The 95.6% of sensitivity, 95.8% of specificity and 96.3% of meningioma tumor image segmentation rate was attained using their improved automated computer methodology in this work. Noreen et al. (2020) devised a brain tumor detection framework using the improved machine learning modeling algorithm in this paper. The segmentation and classification of the various regions of pixels in the brain images were compared significantly with various existing machine learning algorithms in this work. The optimum abnormal detection rate was attained using their improved machine learning model in this work.

Nadeem et al. (2020) analyzed number of taxonomy models and their future challenges were empowered by the taxonomy models. This developed taxonomy models detected meningioma and non-meningioma brain images in this work. The meningioma tumor region segmented output of various tumor detection models was compared and their advantages were highlighted in this work. Ke et al. (2019) modeled the sub space concept for designing the modeling algorithm work flow for the abnormality detection and segmentation in this work. The authors analyzed the automated meningioma tumor detection method using hybrid modeling algorithm in this work. The 93.21% of sensitivity, 94.98% of specificity and 95.98% of meningioma tumor image segmentation rate was accessed using their improved automated computer methodology in this work. Mlynarski et al. (2019) designed a novel meningioma tumor segmentation model using deep learning method in this work. The internal architecture was modified to increase the softmax layer output to produce the higher meningioma detection rate in this work. The authors applied this modified modeling method on different meningioma image dataset and the results were compared and optimum tumor image segmentation rate using their active contour based deep learning model in this work. Jin et al. (2018) designed WMSN on FPGA platform for analyzing their designed pattern and energy consumption rate in this work. Zhou et al. (2016) developed stereo matching method to provide energy efficient WMSN based on the adaptive weighting method. Feng et al. (2003) sensed the data from the various nodes in transmission side of the WMSN system.

3. PROPOSED METHODOLOGIES

An efficient framework to detect and diagnosis of tumor regions in Meningioma image is structured in this paper. The proposed work is structured into two phases as tumor detection phase and tumor diagnosis phase. The tumor detection phase consists of UNet-CNN architecture, which performs both classification and tumor region segmentation process. The features are used for tumor region segmentation process and the computed features are used for the diagnosis of segmented tumor regions into either Early or Severe. This diagnosis phases using UNet and RCNN classification algorithm is depicted in Figure 2.

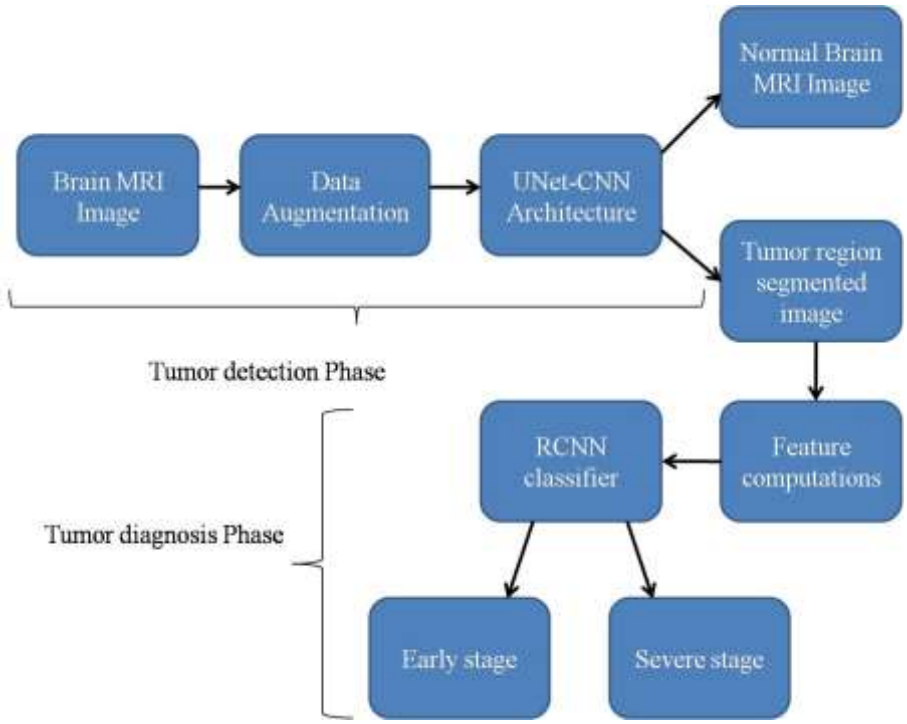

Figure 2: Proposed UNet and RCNN algorithm for tumor detection

3.1. Data augmentation

The proposed UNet architecture necessitates supplementary brain image samples for all two classes. Though the open access dataset consists of number of brain images in both cases, the image counts are not optimum for training or learning the classifier to produce the significant responses. This limitation is resolved by implementing the data augmentation process before the classification process begins. In this work, pixel up shifting and pixel down shifting data augmentation functions are used to produce more reliable and countable images.

3.2. UNet Architecture

In deep leap learning architectures, the internally generated features are created by the internal Convolutional layers in CNN architecture. Then, the abnormality regions are segmented in through the separate tumor segmentation algorithm. This process consumes more time due to two separate architectures for tumor image detection and tumor region segmentation. This drawback can be overcome by proposing UNet architecture (U-shaped deep learning architecture) which combines tumor image detection process and tumor region segmentation process. The proposed UNet architecture for Meningioma tumor segmentation is illustrated in Figure 3. This proposed architecture consists of encoder and decoder part, where both parts contain Convolutional layers and pooling layers with dense layers. The number of filters used in each Convolutional layers are clearly depicted in Figure3 at both encoder and decoder end. In encoder portion this UNet architecture, the encoder network extracts the features from the data augmented images and they have been used for abstract learning process. At the output of each Convolutional layer in encoder part, Rectified Linear Unit (ReLU) is placed to overcome the generated negativity responses. The similar replica architecture is designed in the decoder part of the proposed UNet architecture which performs the reverse operations. The encoder part of the proposed UNet architecture uses down sampling whereas the decoder part of the proposed architecture uses up sampling in each internal layer output.

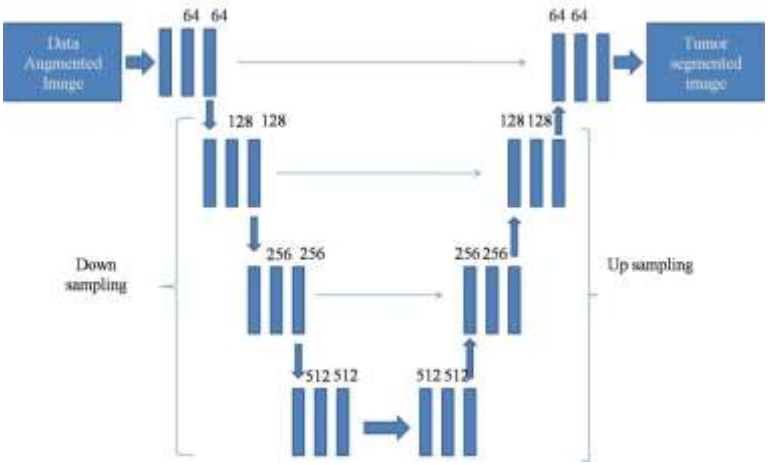

Figure 3: UNet architecture for Meningioma tumor segmentation process

3.3. Tumor diagnosis phase

The textural and statistical features Local Binary Pattern (LBP) and Grey Level Co-occurrence Matrix (GLCM) are computed from tumor region segmented image for the tumor diagnosis process. LBP feature is known as textural feature and GLCM feature is known as statistical features. These features are explained as follows.

3.3.1. LBP

The non-linear binary features are called as LBP and they are computed from the tumor region segmented image. The size of the LBP image is similar with the size of the tumor region segmented image. Therefore, it generates single LBP value for each pixel in the tumor segmented image. The LBP is structured in below steps.

LBP computation Algorithm

Input: Tumor segmented image T(x,y);
Output: LBP feature image;

Start;
Step 1: The tumor segmented image T(x,y) is partitioned by a smaller 3*3 window.
Step 2: Compare the center pixel of the mask window (P_c) with all other surrounding eight neighboring pixels.
Step 3: The neighboring pixel value is changed to 0 if it has the value less than the center pixel P_c.
Step 4: The neighboring pixel value is changed to 1 if it has the value greater than or equals to the center pixel P_c.
Step 5: All these computed eight binary values are converted into decimal value which represents the feature value of the center pixel P_c and the entire LBP computation process is illustrated by the following equation.

$$LBP(P_c) = \sum_{p=1}^{N} 2^{p-1} * f1(P_n - P_c) \quad (1)$$

Where, N is the surrounding pixel counts of the center pixel P_c, P_n is the neighboring pixels.
End;

3.3.2. GLCM features

The statistical features show the non-linear variations of pixels in the tumor segmented image and these features are computed from the GLCM at the angle of orientation 45 degree. The following statistical features are computed from the GLCM for diagnosing the tumor segmented regions into either Early or Severe.

$$Contrast = \sum_{i=1}^{K} \sum_{j=1}^{K} (i-j)^2 S(i,j) \quad (2)$$

$$Energy = \sum_{i=1}^{K} \sum_{j=1}^{K} S(i,j)^2 \quad (3)$$

$$Homogeneity = \frac{\sum_{i=1}^{K} \sum_{j=1}^{K} S(i,j)}{1+|i-j|} \quad (4)$$

$$Correlation = \frac{\sum_{i=1}^{K} \sum_{j=1}^{K} (i-\mu_i)(1-\mu_j) S(i,j)}{\sigma_i \sigma_j} \quad (5)$$

Whereas, $S(i,j)$ the matrix coefficient related with i and j, μ_i and μ_j are the mean values of the matrix coefficient respectively, σ_i and σ_j are the standard deviations of the matrix coefficient respectively.

3.3.3. Region based CNN (RCNN) classifier

The computed statistical and textural features from the tumor region segmented image are used in this work for diagnosing the tumor regions into 'Early' or 'Severe' using RCNN classification architecture. The CNN classifier which is integrated with region proposal layers is known as RCNN classifier. The author Girshick et al. (2016) used RCNN classifier for object detection applications using the internal features generated by the CNN layers. This property of object detection in an image can be modified to diagnose the segmented tumor into either Early or Severe. The region proposal layer in conventional RCNN architecture is replaced by the two channel CNN architectures. The proposed RCNN architecture is depicted in Figure 4.

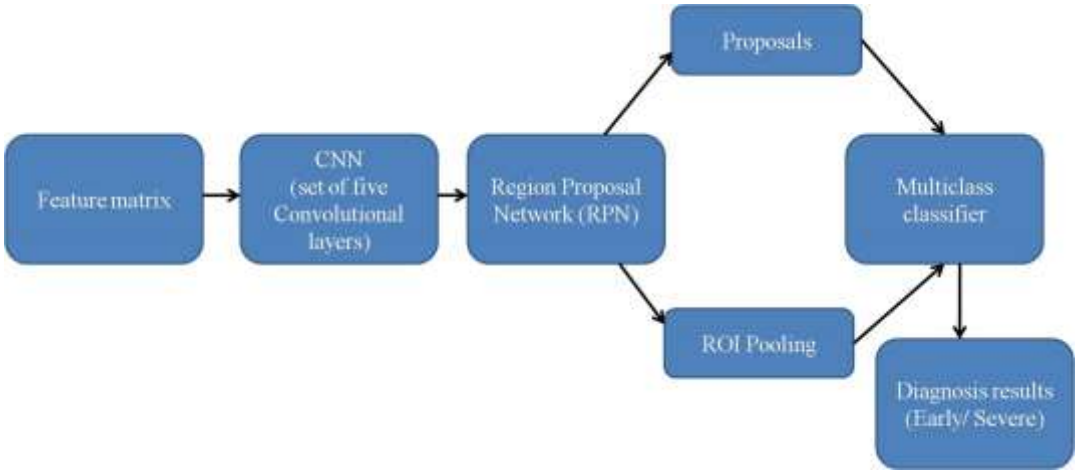

Figure 4: Proposed RCNN structure for severity classifications

The RPN is a set of CNN which is used to predict the object bounds and scores of the object bounds at each feature value point. The numbers of higher end region proposals are generated by RPN. This RPN can be functioned either sliding window approach or selective search approach. In case of sliding window approach in RCN the regions are generated for each feature value point with respect to its coordinates and scale. This increases the computational complexity and hence this approach consumes more time to generate the proposals. In order to overcome such limitations, selection search approach is used in RPN to generate the number of proposals for each feature value. The generated proposals along with Region Of Interest (ROI) are classified by the multiclass classifier, which produces the diagnosis results as either Early or severe, as illustrated in Figure4.

Figure 5 (a) shows the Meningioma images and Figure 5(b) shows the tumor segmented images by proposed method.

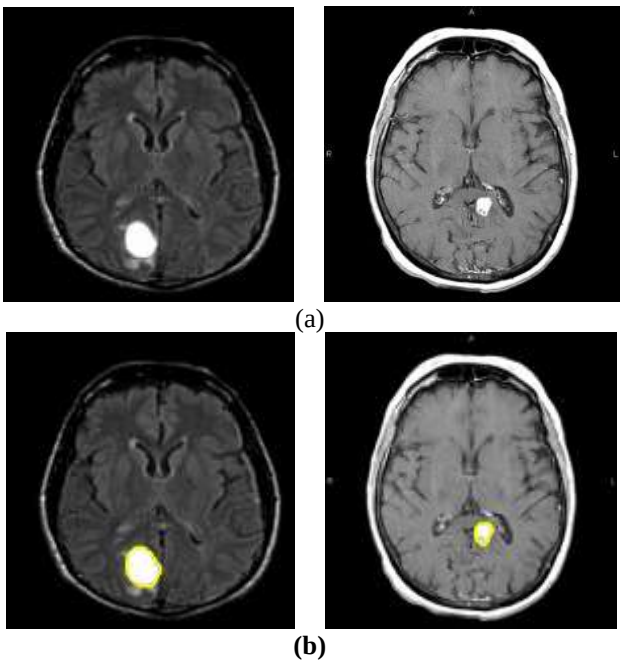

(a)

(b)

Figure 5: (a) Meningioma images (b) Tumor segmented images

Figure 6(a) is the severe Meningioma brain image and Figure 6(b) is the Early Meningioma brain image.

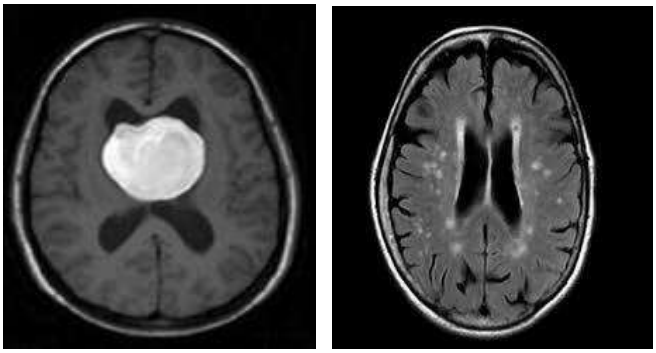

(a) **(b)**

Figure 6: (a) Severe Meningioma (b) Early Meningioma

4. RESULTS AND DISCUSSIONS

The proposed UNet-RCNN classification approach for Meningioma tumor segmentation process is simulated and tested on Nanfang University (NU) dataset [10], which was constructed and maintained by Nanfang hospital, China. This dataset can be found as open access website [10] and this website does not require any licensing options to use the materials or data used in any other formats. For the experimental purpose, 571 meningioma and 850 healthy brain images are accessed from this Nanfang dataset and used as the input for the proposed meningioma tumor segmentation system. Also, Kaggle dataset [5] is used in this work to analyze the performance efficiency of the proposed method. For the experimental purpose, 300 meningioma brain images and 350 non-meningioma brain images or healthy brain images are accessed from this Nanfang dataset and used as the input for the proposed meningioma tumor segmentation system.

The below equations describes the performance of Meningioma detection method.

$$Sensitivity\ Index\ Rate\ (SEIR) = \frac{TP}{TP+FN} \quad (6)$$

$$Specificity\ Index\ Rate\ (SPIR) = \frac{TN}{TN+FP} \quad (7)$$

$$Accuracy\ Rate\ (AR) = \frac{TP+TN}{TP+TN+FP+FN} \quad (8)$$

$$Precision\ (PR) = \frac{TP}{TP+FP} \quad (9)$$

$$F1-Score\ (FS) = \frac{2*TP}{2*TP+FP+FN} \quad (10)$$

Where, TP, TN represents detected tumor and non-tumor pixels with respect to true pixels, FP, FN represents detected tumor and non-tumor pixels with respect to false pixels.

Table 1 is the effective analysis of the proposed CCNN on NU dataset images.

Table 1: Effective analysis of proposed CCNN on NU dataset

Meningioma image orders	Performance measures in %				
	SEIR	**SPIR**	**AR**	**PR**	**FS**
1	97.8	99.3	99.3	98.5	98.6
2	98.3	98.2	98.7	98.9	98.9
3	98.7	98.6	98.1	99.2	99.3
4	98.6	98.7	98.6	99.1	99.2
5	99.1	98.5	98.4	98.7	99.1
6	98.6	98.4	98.5	98.9	98.7
7	98.4	98.9	99.3	99.3	98.9
8	98.7	98.2	99.1	98.6	99.3
9	98.9	98.1	98.5	98.5	98.6
10	99.3	99.3	98.3	99.1	98.7
Average	**98.64**	**98.62**	**98.68**	**98.88**	**98.93**

Figure 7 is the graphical simulation layout of the simulation results.

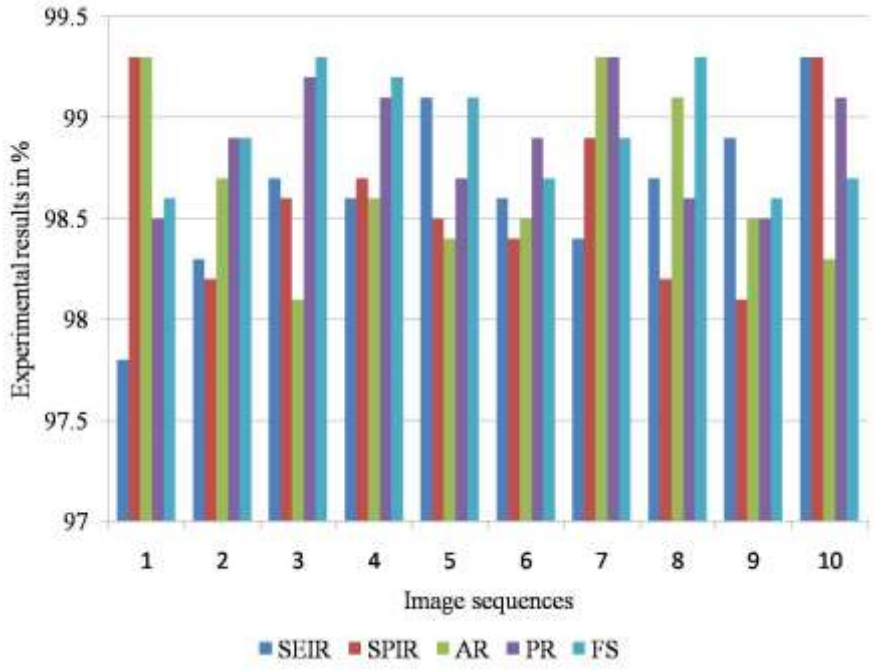

Figure 7 Graphical simulation lay out of the simulation results

Table 2 is the effective analysis of the proposed CCNN on Kaggle dataset images.

Table 2: Effective analysis of proposed CCNN on Kaggle dataset

Meningioma image orders	Performance measures in %				
	SEIR	**SPIR**	**AR**	**PR**	**FS**
1	98.3	98.3	98.6	98.8	98.8
2	98.7	99.2	98.5	98.6	98.6
3	98.1	99.5	98.9	99.3	99.1
4	98.7	99.1	99.3	99.1	99.3
5	98.6	98.7	99.1	99.8	98.7
6	98.4	98.9	98.6	98.6	98.3
7	98.5	98.6	98.8	98.3	98.7
8	99.3	98.8	98.3	98.8	98.5
9	99.1	98.9	98.2	98.2	98.9
10	99.3	99.2	99.8	98.9	98.3
Average	**98.7**	**98.92**	**98.81**	**98.84**	**98.72**

Figure 8 is the graphical simulation layout of the simulation results (for Kaggle).

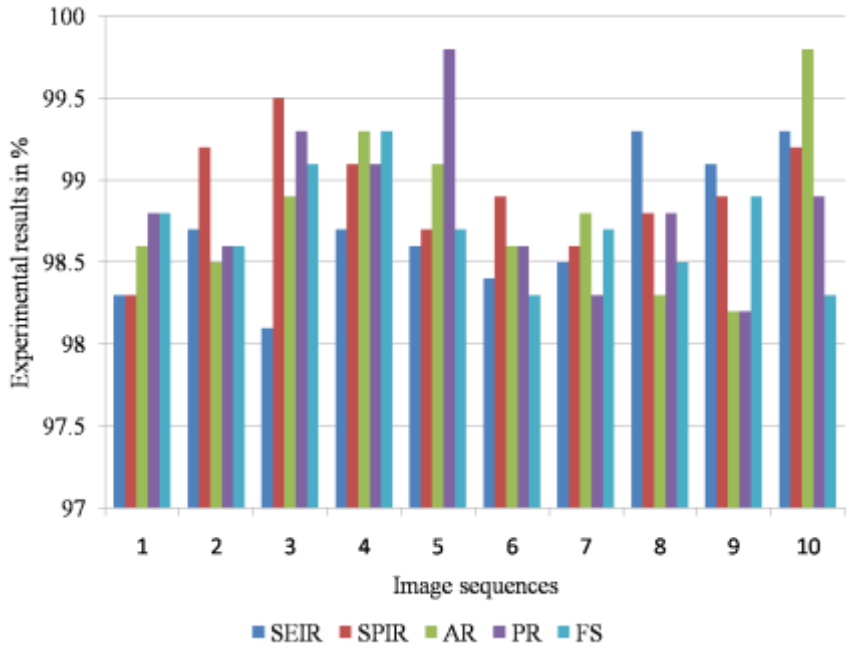

Figure 8 Graphical simulation lay out of the simulation results (Kaggle)

Table 3 shows the comparative performance measures between the two established brain image datasets.

Table 3: Comparative performance measures

Parameters	Datasets	
	NU dataset	Kaggle dataset
SEIR	98.64	98.7
SPIR	98.62	98.92
AR	98.68	98.81
PR	98.88	98.84
FS	98.93	98.72

Table 4 is comparative measurement on NU dataset.

Shanaka Ramesh et al. (2021) obtained 95.9% of sensitivity, 96.1% of specificity and 96.7% of meningioma tumor, Laukamp et al. (2020) obtained 95.6% of sensitivity, 95.8% of specificity and 96.3% of meningioma tumor image, Ke et al. (2019) obtained 93.21% of sensitivity, 94.98% of specificity and 95.98% of meningioma tumor and Mlynarski et al. (2019) obtained 93.2% of sensitivity, 94.4% of specificity and 95.7% .

Table 4: Proposed work Comparisons with others (for NU case)

Methodology	SEIR	SPIR	AR	PR	FS
Proposed CCNN approach (in this paper)	**98.64**	**98.62**	**98.68**	**98.88**	**98.93**
Shanaka Ramesh et al. (2021)	95.9	96.1	96.7	95.2	96.9
Laukamp et al. (2020)	95.6	95.8	96.3	96.9	96.4
Ke et al. (2019)	93.21	94.98	95.98	95.9	96.4
Mlynarski et al. (2019)	93.2	94.4	95.7	96.9	95.9

Table 5 is comparative measurement on Kaggle dataset.

Table 5: Proposed work Comparisons with others (for Kaggle case)

Methodology	SEIR	SPIR	AR	PR	FS

Proposed CCNN approach (in this paper)	**98.7**	**98.92**	**98.81**	**98.84**	**98.72**
Shanaka Ramesh et al. (2021)	95.29	94.67	94.19	94.29	94.85
Laukamp et al. (2020)	94.39	94.67	94.28	95.03	95.01
Ke et al. (2019)	93.29	93.28	94.10	94.39	94.96
Mlynarski et al. (2019)	94.29	94.67	94.29	94.10	94.39

The segmented tumor pixels in meningioma brain images are now compressed using Huffman encoding method. The encoded and compressed pixels in meningioma image are transferred through the wireless multimedia sensor networks to the remote unit in this work. At the receiver side of wireless multimedia sensor networks, the compressed tumor pixels are received and they are decompressed using inverse Huffman decoding method.

5. CONCLUSIONS

In this work, the Meningioma tumor images are classified and the tumor regions are segmented using UNet-CNN classification algorithm. The segmented tumor regions in Meningioma brain images are further diagnosed using RCNN classifier. This proposed tumor segmentation and diagnosis approach tested on two different NU and Kaggle datasets to validate the experimental results. The proposed CCNN approach for Meningioma tumor detection on NU dataset obtains 98.64% SEIR, 98.62% SPIR, 98.68% AR, 98.88%PR and 98.93% FS. The proposed CCNN approach for Meningioma tumor detection on Kaggle dataset obtains 98.7% SEIR, 98.92% SPIR, 98.81% AR, 98.84%PR and 98.72% FS. Finally, the segmented tumor pixels in meningioma brain images are now compressed using Huffman encoding method.

REFERENCES

1 Ali S., Li J., Pei Y., Khurram R., Rehman K., Mahmood T. “A comprehensive survey on brain tumor diagnosis using deep learning and emerging hybrid techniques with multi-modal MR image,” *Arch. Comput. Methods Eng.*, 2022; 2022: 1–26.

2 Feng W, Code B, Kaiser E, et al, “Panoptes: A Scalable Architecture for Video Sensor Networking Application,” *Proc. the ACM Int’l Conference on Multimedia*, New York, 2003; 151–67.

3 Jin, S., Yuanzhi, W. & Yining, S. “Design and implementation of wireless multimedia sensor network node based on FPGA and binocular vision,” *J Wireless Com Network*, 2018; 163.

4 Kaggle dataset, Available at: https://www.kaggle.com/datasets/navoneel/brain-mri-images-for-brain-tumor-detection

5 Ke Q., Zhang J., Wei W., Damaševičius R., Woźniak M. “Adaptive independent subspace analysis of brain magnetic resonance imaging data,” *IEEE Access*, 2019; 7:12252–61.

6 Laukamp K.R., Pennig L., Thiele F. et al., “Automated meningioma segmentation in multiparametric MRI: comparable effectiveness of a deep learning model and manual segmentation,” *Clinical Neuroradiology*, 2020.

7 Mlynarski P., Delingette H., Criminisi A., and Ayache N., “Deep learning with mixed supervision for brain tumor segmentation,” *Journal of Medical Imaging*, 2019; 6(3): 1-8.

8 Nadeem M. W., Al Ghamdi M. A., Hussain M. et al., “Brain tumor analysis empowered with deep learning: a review, taxonomy, and future challenges,” *Brain Sciences*, 2020; 10(2): 1–33.

9 Nanfang University (NU) dataset, Available at: https://doi.org/10.6084/m9.figshare.1512427.v5.

10 Noreen N., Palaniappan S., Qayyum A., Ahmad I., Imran M., and Shoaib M., “A deep learning model based on concatenation approach for the diagnosis of brain tumor,” *IEEE Access*, 2020; 8: 55135–44.

11 Shanaka Ramesh, Gunasekara, H. N. T. K. Kaldera, Maheshi B. Dissanayake, "A Systematic Approach for MRI Brain Tumor Localization and Segmentation Using Deep Learning and Active Contouring", Journal of Healthcare Engineering, 2021; 2021: 1-13.

12 Zhou W.W., Jin W.G., “Novel Stereo Matching algorithm for adaptive weight census transform,” *Comput Eng Appl*., 2016; 52(16): 192–7.